JOURNAL OF GUIDANCE, CONTROL, AND DYNAMICS
Vol. 21, No. 6, November–December 1998

Applied Active Control for a Nonlinear Aeroelastic Structure

Jeffry J. Block* and Thomas W. Strganac†
Texas A&M University, College Station, Texas 77843-3141

Linear and nonlinear aeroelastic response is examined using a unique test apparatus that allows for experiments of plunge and pitch motion of a wing with prescribed stiffness characteristics. The addition of a control surface, combined with an active control system, extends the stable flight region. Unsteady aerodynamics are modeled with an approximation to Theodorsen's theory appropriate for the low reduced frequencies associated with the experiment. Incorporated with a full-state feedback control law, an optimal observer is utilized to stabilize the system above the open-loop flutter velocity. Coulomb damping and hardening of the pitch stiffness are included to examine nonlinear control behavior. The nonlinear model is tested using the control laws developed from an extension of linear theory. Each model is simulated using MATLAB® and compared with experimental results of the active control system. Excellent correlation between theory and experiment is achieved. Using an optimal observer and full-state feedback, the linear and nonlinear systems are stabilized at velocities that exceed the open-loop flutter velocity. Limited control is achieved when the system is undergoing limit cycle oscillations.

Nomenclature

a = nondimensional distance from the midchord to the elastic axis
b = semichord of wing (reference length)
$C(k)$ = Theodorsen's function
c = nondimensional distance from midchord to control surface hinge
c_h = plunge degree of freedom structural damping coefficient
c_α = pitch degree of freedom structural damping coefficient
e = nondimensional distance from midchord to control surface leading edge
g = acceleration due to gravity
h = plunge displacement coordinate
I_α = mass moment of inertia about the elastic axis
K = full-state feedback gains
k = reduced frequency $(b\omega/u_\infty)$
k_h = plunge degree of freedom structural spring constant
k_α = pitch degree of freedom structural spring constant
L = estimator gains
$L(t)$ = lift of the wing
M_f = friction moment caused by Coulomb damping
$M(t)$ = moment of the wing about the elastic axis
m = mass of the wing
Q = state weighting matrix
$\bar{Q}$ = process noise covariance
R = control weighting matrix
$\bar{R}$ = measurement noise covariance
u = freestream velocity
x_α = nondimensional distance between elastic axis and the center of mass
α = pitch displacement coordinate
β = control surface deflection coordinate
ΔA = difference in peak amplitudes of the free vibration
μ_h = static coefficient of friction in the plunge direction
μ_α = static coefficient of friction in the pitch direction
ρ = density of air
ω = frequency of motion

Received Sept. 11, 1997; revision received June 3, 1998; accepted for publication June 4, 1998.

*Graduate Research Assistant, Department of Aerospace Engineering. Member AIAA.
†Associate Professor, Department of Aerospace Engineering. Associate Fellow AIAA.

Introduction

AEROELASTICITY is the interaction of structural, inertial, and aerodynamic loads. Combined, these loads may cause aircraft components to become unstable. Active suppression of aeroelastic instabilities, such as flutter, divergence, and control reversal, will lead to improved performance. Many control strategies have been applied to suppress flutter or to control unacceptable wing motion. Lyons et al.[1] investigated full-state feedback with a Kalman estimator for the purpose of flutter suppression. Their theoretical model was relatively simple and required only eight states. Mukhopadhyay et al.[2] and Gangsaas et al.[3] used high-order models and developed methods for reducing these higher-order systems to show the practicality of such controllers. These control systems implemented estimators to describe unmeasured states and used output feedback as the control method. Karpel[4] compared the aerodynamic descriptions of Lyons et al.[1] to develop partial-state feedback controllers. He used pole placement techniques to develop the control laws for flutter suppression and gust alleviation.

Horikawa and Dowell[5] performed flutter analysis with control, employing proportional gain feedback methods developed from root locus plots. They used a steady aerodynamic, two degree-of-freedom structural model to develop several types of feedback. The approach directly feeds one of four variables to the control surface through a proportional gain. A recent investigation of flutter suppression by Heeg[6] increased the flutter velocity by 20%. The work involved a small wing model mounted on spring tines to simulate the bending and torsion modes. Four piezoelectric plates were mounted to control the bending mode. Heeg's analysis employs a classic approach for control by using root locus plots to derive proportional gain feedback control laws.

In a study by Lin,[7] Lazarus et al.,[8] and Lazarus,[9] a typical section model was analyzed. The study included control of the bending and torsion modes by piezoelectric materials and additional control with leading- and trailing-edge flaps. They showed that direct control through piezoelectrics was most efficient. Their design approach implemented full-state feedback with an estimator. Lazarus conducted experimental analysis to validate the typical section model. This structure and control scheme was designed for wind-tunnel disturbance rejection, gust alleviation, and flutter suppression.

These researchers have shown that linear theory is applicable for elaborate control systems in many cases. Unfortunately, as flight control systems and the associated performance of current military and civilian aircraft become increasingly complicated, the needs for more sophisticated aeroservoelastic models also increase. Most systems contain nonlinearities that are either neglected by the designer or linearized within the equations of motion. Recently, researchers have studied in detail the nonlinearities inherent in aeroelastic systems.

Before describing these research efforts, it is important to discuss common nonlinearities that may occur in aeroelastic systems. As a control example, saturation occurs when an increasing input into a system will no longer increase the output of the system. This nonlinearity occurs in actuators when their operational limits are exceeded. Free-play nonlinearities occur in control surface linkages or hinges in which the surface will not move until the magnitude of the input exceeds a certain value. Hysteresis occurs in systems when friction loads affect linkage dynamics or when connections (i.e., rivets) slip in wing structures. A stiffness nonlinearity may also occur in many structures. For instance, nonlinear stiffnesses are observed in large bending deflections of wings and rotor blades or in control systems that become increasingly harder to deflect (nonlinear proportionality) as they are moved farther from the neutral position.

Several advanced fighter aircraft have experienced limit cycle oscillations (LCOs) for certain attached wing store configurations.[10,11] The mechanism that leads to these LCOs is not understood, but possible explanations under study include aerodynamic and/or structural nonlinearities. Stiffness tests show evidence of a spring-hardening nonlinearity in the wing torsional mode. This type of nonlinearity will lead to LCO behavior similar to that described herein.

Woolston et al.[12] investigated nonlinearities in structural stiffness and control surface linkages. They created several models with free-play, hysteresis, cubic-hardening, and cubic-softening nonlinearities in the torsional mode. For general wing motion, they observed that the flutter velocity decreased as the initial disturbance increased, and that the stability of the system was highly dependent on the magnitude of the initial condition. A cubic-softening spring stiffness lowered the flutter velocity. They also noted that cubic hardening caused limit cycle oscillations rather than flutter at velocities above the open-loop flutter velocity.

Breitbach[13] showed that a poor agreement between theory and experiment in flutter is most likely due to the presence of nonlinear structural stiffness. He also presented a detailed examination of many types of nonlinearities that may affect aeroelastic systems. Tang and Dowell[14] introduced a free-play nonlinearity in the torsional stiffness and examined the nonlinear aeroelastic response. For various initial conditions, they created maps of the system response to describe locations of periodic limit cycles, chaotic motion, and divergent motion. They concluded that limit cycle motion is dependent upon freestream velocity, initial pitch condition, magnitude of the free-play nonlinearity, and initial conditions.

Lee and LeBlanc[15] performed a numerical analysis of a nonlinear wing model using a time-marching scheme that simulated aeroelastic motion. Softening and hardening cubic stiffnesses were examined by varying the mass ratio, increasing the distance between the elastic axis and the center of mass, and varying the ratio of the plunge frequency to pitch frequency. For the spring-softening case, unstable motion was encountered below the linear flutter speed for nearly every parameter examined; however, increasing the nonlinearity and increasing the mass ratio tended to make the system more unstable at lower velocities. For the spring-hardening case, limit cycle oscillations were always present instead of flutter. Varying the parameters for the spring-hardening case affected the amplitudes of the limit cycle oscillations.

In this paper, an unsteady aerodynamic model is developed with an approximation to Theodorsen's function, and an observer, based upon the Kalman estimator, is used to estimate the augmented state system. Theodorsen[16] developed an unsteady aerodynamic theory that accounts for the lag effects of the unsteady aerodynamics for different frequencies. Theodorsen and Garrick[17] used this method to compare theoretical predictions of flutter velocity and frequency with experimental results. The method assumes harmonic motion of the wing and provides a widely accepted approach to predict the flutter velocity and frequency. The need to simulate wing motion in unsteady aerodynamic flowfields led to the approximations of Theodorsen's function by Wagner and Jones (see Ref. 18). With these approximations, the equations of motion are more easily solved to predict aeroelastic response.

Following the developments by Wagner and Jones, several researchers attempted to further understand the unsteady motion of an airfoil. Lyons et al.[1] transformed Jones' approximation into the Laplace domain and augmented the states of the system to account for the lag terms in the aerodynamics. This approach facilitated control law development. To describe Wagner's function and Theodorsen's function in the frequency domain, Vepa[19] developed a Padé approximation technique. He showed this method to be valuable for arbitrary small motions of a thin wing. Edwards et al.[20] compared the methods of Lyons and Vepa and contributed to the development by separating the aerodynamics into rational and nonrational components. The nonrational part was isolated because it cannot be written as a ratio of polynomials. Edward's method, which also applied to arbitrary small motion of a wing, reduced the number of augmented states previously required to model the unsteady aerodynamics.

These researchers have developed models for exploring nonlinear aeroelasticity and have also attempted to describe the motion with time-marching solutions and describing function analysis. However, there are limited efforts to examine nonlinear aeroelasticity and active control strategies. The experiment at Texas A&M University permits a prescribed linear or nonlinear structural stiffness. With nonlinear structural stiffness, the model exhibits limit cycle oscillations.[21] Various full-state feedback control laws have been tested on the structure with the addition of a control surface. Tests of the linear structural model and nonlinearities are examined. Control is demonstrated using the linear controller. The work presented herein combines active flutter control with nonlinear aeroelasticity.

Theory

A wing section with a control surface is mounted to permit plunge (h) and pitch (α) motion about the elastic axis as shown in Fig. 1. The mass, inertia, damping, stiffness, and aerodynamic loads are per unit span. The control surface hinge is located at the leading edge of the control surface, thus e is equal to c in all derivations that follow. The motion of the system, without control surface dynamics, may be described by

$$\begin{bmatrix} m & mx_\alpha b \\ mx_\alpha b & I_\alpha \end{bmatrix} \begin{Bmatrix} \ddot{h} \\ \ddot{\alpha} \end{Bmatrix} + \begin{bmatrix} c_h & 0 \\ 0 & c_\alpha \end{bmatrix} \begin{Bmatrix} \dot{h} \\ \dot{\alpha} \end{Bmatrix} + \begin{bmatrix} k_h & 0 \\ 0 & k_\alpha \end{bmatrix} \begin{Bmatrix} h \\ \alpha \end{Bmatrix} = \begin{Bmatrix} -L(t) \\ M(t) \end{Bmatrix} \tag{1}$$

where lift $L(t)$ and moment $M(t)$ represent the unsteady aerodynamics that depend upon position, velocity, acceleration, and time. The lift and moment act at the elastic axis of the wing. Theodorsen[16]

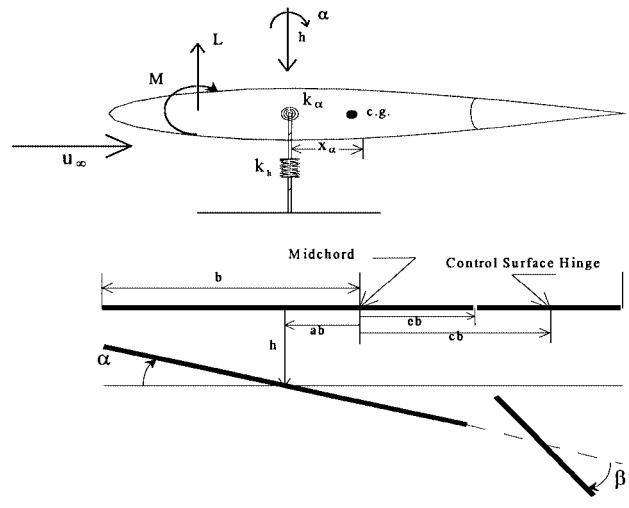

Fig. 1 Aeroelastic system modeled as a wing section with two degrees of freedom with an attached full span control surface.

derived the lift per unit span and moment per unit span, assuming harmonic motion of the airfoil, of the form

$$-L(t) = -\rho b^2(u\pi\dot{\alpha} + \pi\ddot{h} - \pi ba\ddot{\alpha} - uT_4\dot{\beta} - T_1 b\ddot{\beta}) - 2\pi\rho ubC(k)\left[u\alpha + \dot{h} + b\left(\tfrac{1}{2} - a\right)\dot{\alpha} + (1/\pi)T_{10}u\beta + b(1/2\pi)T_{11}\dot{\beta}\right] \tag{2}$$

$$M(t) = -\rho b^2\left\{\pi\left(\tfrac{1}{2} - a\right)ub\dot{\alpha} + \pi b^2\left(\tfrac{1}{8} + a^2\right)\ddot{\alpha} + (T_4 + T_{10})u^2\beta + \left[T_1 - T_8 - (c-a)T_4 + \tfrac{1}{2}T_{11}\right]ub\dot{\beta} - [T_7 + (c-a)T_1]b^2\ddot{\beta} - a\pi b\ddot{h}\right\} + 2\rho ub^2\pi\left(\tfrac{1}{2} + a\right)C(k)\left[u\alpha + \dot{h} + b\left(\tfrac{1}{2} - a\right)\dot{\alpha} + (1/\pi)T_{10}u\beta + b(1/2\pi)T_{11}\dot{\beta}\right] \tag{3}$$

The functions T are described by Theodorsen[16] and are dependent upon the elastic axis location and the control surface hinge location.

To implement the control surface dynamics with the equations of motion in Eq. (1), the control surface dynamics are assumed to be that of a second-order system such that the dynamics will not affect the coupling of the plunge and pitch motion of the wing section. These dynamics are represented by the second-order oscillator[22]

$$\ddot{\beta} + 50\dot{\beta} + 2500\beta = 2500\beta_{\text{com}} \tag{4}$$

where β_{com} is the control variable for the entire system. The combined equations of motion are represented by

$$[M]\{\ddot{X}\} + [C]\{\dot{X}\} + [K]\{X\} = [D]\{\beta_{\text{com}}\} \tag{5}$$

which now include the dynamics of the control surface.

The function $C(k)$, found in the lift and moment terms of Theodorsen's function, contains real and imaginary terms of the form[16,18]

$$C(k) = F(k) + iG(k) \tag{6}$$

where $F(k)$ and $G(k)$ are composed of Bessel functions. Jones (see Ref. 18) developed an approximation to Theodorsen's function that simplifies mathematical calculations. The approximation, which may also be represented in the Laplace domain, is described by

$$C(k) = 1 - \frac{0.165}{1 - (0.0455i/k)} - \frac{0.335}{1 - (0.3i/k)} \tag{7}$$

Six new states are added to the system to incorporate this approximation into the lift and moment equations. The new states account for the aerodynamic lag due to the second and third terms of Eq. (7) and are defined in the Laplace domain by

$$\hat{X}(s) = \frac{s}{s + 0.0455(u/b)}X(s), \qquad \bar{X}(s) = \frac{s}{s + 0.3(u/b)}X(s) \tag{8}$$

where $X(s)$ consists of the plunge, pitch, and control surface states. After expanding and converting Eq. (8) to the time domain, the resulting equations are

$$\dot{\hat{X}} - \dot{X} + 0.0455(u/b)\hat{X} = 0, \qquad \dot{\bar{X}} - \dot{X} + 0.0455(u/b)\bar{X} = 0 \tag{9}$$

Substitution of the numerators in Eq. (7) are made for $C(k)$ in the equations of motion and are applied to the new states, $\hat{X}(s)$ and $\bar{X}(s)$. The equations of motion (5), with the redefined unsteady aerodynamics, are rewritten as

$$[M_1]\{\ddot{X}\} + [C_1]\{\dot{X}\} + [C_2]\{\dot{\hat{X}}\} + [C_3]\{\dot{\bar{X}}\} + [K_1]\{X\} + [K_2]\{\hat{X}\} + [K_3]\{\bar{X}\} = [D_1]\{\beta_{\text{com}}\} \tag{10}$$

The six additional equations from Eq. (9) are combined with Eq. (10) and placed in state-space form such that

$$\{\dot{X}\} = [A]\{X\} + [B]\{U\} \tag{11}$$

with the output equations

$$\{Y\} = [I_{2\times 2} \quad 0_{2\times 10}]\{X\} = [Z]\{X\} \tag{12}$$

This system consists of 12 states, of which only plunge and pitch displacements are measured. The remaining 10 states are determined with a state estimator.

Assuming the system is stabilizable, a full-state feedback control law can be derived to stabilize the closed-loop system. The feedback gains may be determined using various control methodologies (e.g., a pole-placement technique) or by optimizing a performance index with a linear quadratic regulator (LQR) approach. In this paper, we adopt the LQR method to stabilize the system. Specifically, the following performance index for our aeroelastic model is selected:

$$J = \int_0^\infty \left[\left(\frac{h}{h_{\max}}\right)^2 + \left(\frac{\alpha}{\alpha_{\max}}\right)^2 + \left(\frac{\beta}{\beta_{\max}}\right)^2\right]\mathrm{d}t \tag{13}$$

This particular index normalizes the maximum values of the states and inputs, and the restraints on the index will keep the maximum amplitudes to a minimum. After choosing the state and control weighting matrices that describe the performance index, the optimal feedback gains are found by solving the algebraic Ricatti equation (see Ref. 23). However, the chosen performance index is only a first approximation for the weighting, and the system should be examined at various conditions to scale the gains. The weightings must be varied until an acceptable set of feedback gains are determined. Specifically, the weightings must be chosen so that the control law does not saturate in practice.

The complete system consists of 12 states, 1 input (β_{com}) and 2 outputs (h, α). It is most ideal to implement a full-state feedback control scheme, but because all of the states are not measurable, this is not feasible. Instead, a state observer will be used to estimate those states that are not measurable. In this paper, we employ the well-known Kalman estimator to be used with the LQR controller. A detailed discussion of the Kalman estimator is found in various texts (e.g., see Ref. 23).

Although the derived estimator is optimal for the given weightings, these weightings may not be optimal for the system. The control system is based on the measurements from the sensors and the integration of the estimator equations of motion. If the model of the system is not accurate, then as the actual states lead to one solution, the estimated states may potentially lead to a contrary solution. Therefore, it is important that the system model be accurate and that substantial testing of the estimator is complete before the final design of the aeroelastic control system.

Two nonlinearities are considered to better describe the model and actual structural response. First, Coulomb damping, a friction force that opposes the motion of the system, is observed in the response of the plunge and pitch motion. Previous models have been described with strictly viscous damping models, which suggests a logarithmic decay. The viscous damping terms c_h and c_α are neglected when Coulomb damping is applied. In this study, Coulomb damping is used to predict linear flutter velocities as well as limit cycle motions. The second nonlinearity is a pitch-hardening stiffness that is associated with a nonlinear cam. The nonlinear stiffness is presented in Table 1. This stiffness term was derived by O'Neil[21] and is introduced into the experiments by a unique experiment test apparatus that permits a prescribed linear or nonlinear stiffness response.

The linear response possesses a viscous form of structural damping in both the plunge and pitch degrees of freedom. This damping is identified by measuring the logarithmic decay during free vibration experiments. The pitch degree of freedom is restrained for measurements of the plunge damping, and the plunge degree of freedom is restrained for measurements of the pitch damping. With validation that the damped free vibration is indeed logarithmic, the

Table 1 Aeroelastic experiment parameters

Constants	Values
a	-0.8424
b	0.135
Span, m	0.6
m_w, kg	1.662
m_t, kg	12.387
r_{cg}, m	0.066
I_α, kg m^2	0.065
k_h, N/m	2844.4
k_α (linear), N-m/rad	3.525
k_α (nonlinear), N-m/rad	$2.82(1 - 22.1\alpha + 1315.5\alpha^2 - 8580\alpha^3 + 17289.7\alpha^4)$
c_h, kg/s	27.43
c_α, kg m^2/s	0.036
μ_h	0.0221
μ_α	0.0113

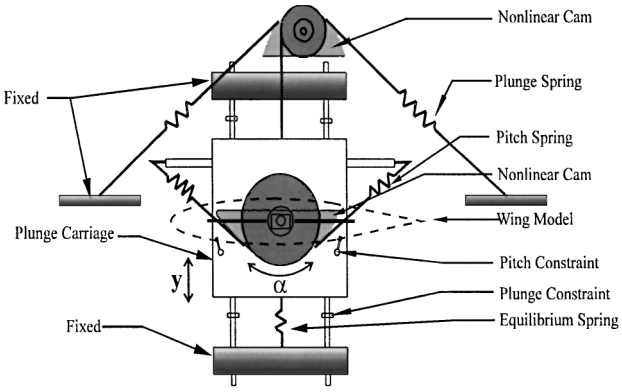

Fig. 2 Schematic view of the experimental setup (upper view); the wing is mounted vertically in the 2 × 3 ft low-speed wind tunnel (lower view).

log-decrement method is used to calculate the damping ratio ζ for each degree of freedom.

The nonlinear response possesses both viscous and Coulomb damping. Although viscous damping appears as a logarithmic decay, Coulomb damping appears as a linear decay. In the equations of motion, viscous damping is represented by a linear term proportional to the velocity. However, Coulomb damping is defined by a force opposing the motion of the system, and once the friction force is greater than the restoring force, the system motion will stop. The equations for the plunge and pitch Coulomb forces are defined, respectively, by

$$F_h = \mu_h mg(|\dot{h}|/\dot{h}), \qquad F_\alpha = \mu_\alpha M_f(|\dot{\alpha}|/\dot{\alpha}) \tag{14}$$

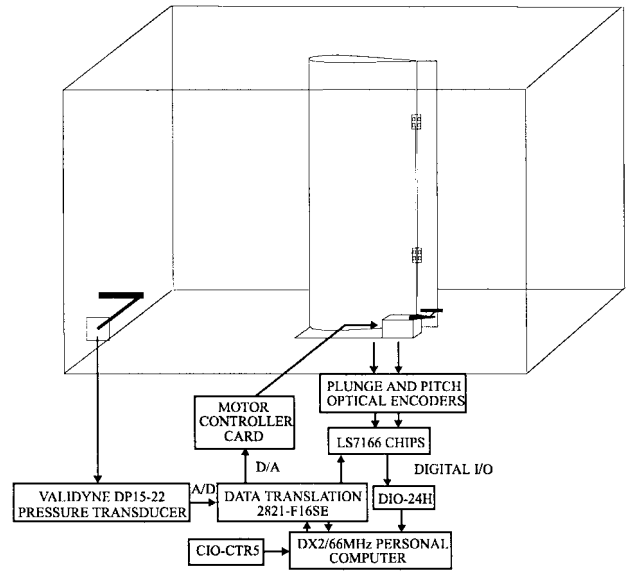

Fig. 3 Flow chart of the active control system.

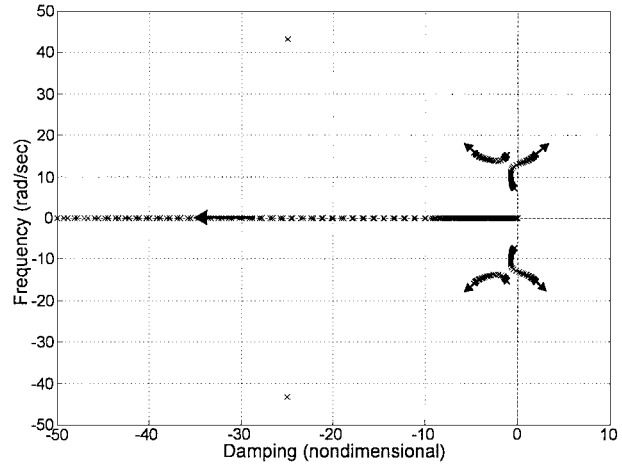

Fig. 4 Root-locus plot of the aeroelastic equations provides stability characteristics with respect to freestream velocity.

A frictional moment M_f is due to the mass offset of the nonlinear pitch cam. To determine the coefficients of friction, the following equation is used:

$$\mu = (\Delta A/4g)\omega_n^2 \tag{15}$$

When the nonlinear cams are applied to the system, the free vibration possesses more Coulomb damping than viscous damping. Thus, viscous damping is used solely in the linear system simulations, and the Coulomb damping is included for the nonlinear simulations. Table 1 summarizes the structural constants for the system.

Experiment

The aeroelastic model was tested in Texas A&M University's 2 × 3 ft wind tunnel. This tunnel has a maximum operating speed of 150 ft/s (45 m/s), which is well beyond the designed flutter boundary of the model. The wing section (see Figs. 1 and 2) is mounted vertically in the tunnel and is the only component exposed to the flow. Motion in the plunge and pitch directions is dictated by a twin-cam system. The maximum plunge deflection is ±0.134 ft (±0.04 m), and the maximum pitch angle is ±28 deg. The combination of the spring stiffness and the cam shape provides the prescribed linear or nonlinear response. A control surface and motor are designed for easy attachment and removal. The control surface chord is 20% of the full chord and is a full-span surface.

The aerodynamic loads on the control surface require a high torque motor. Also, a minimal size is desired because the motor

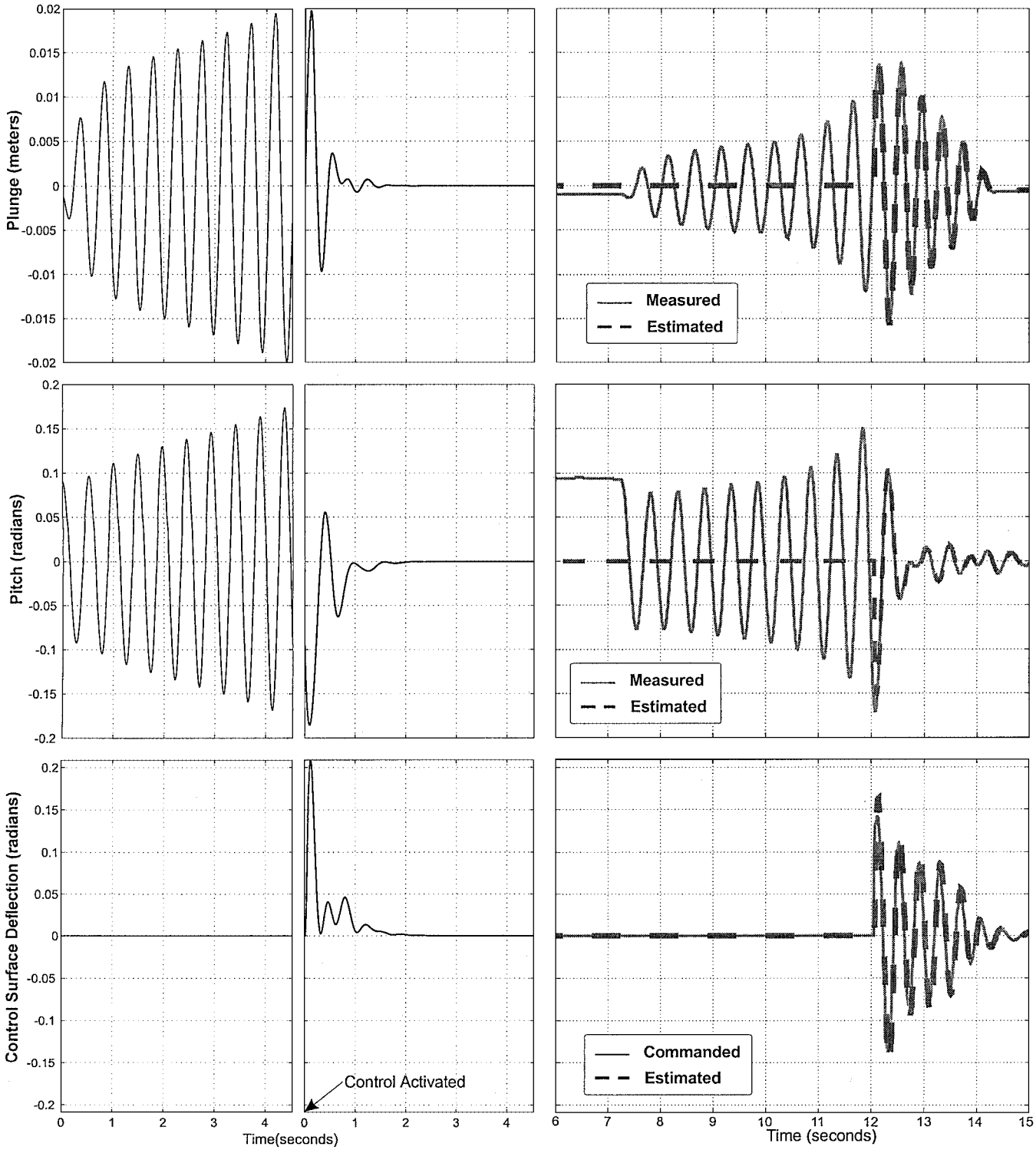

Fig. 5 Predictions of controlled response for the linear system at u_∞ = 15.5 m/s are shown in the left-side view. Measurements of controlled response are shown in the right-side view. Lower view shows control surface deflection.

is placed externally on the wing. The Futaba FPS-134 servomotor is used as it is small in size, will deliver up to 112.6 oz-in. (0.07951 N-m) of torque, and has an embedded controller board that directs its motion. This controller requires a continuous square wave signal to define the intended position. An electric circuit board has been developed to drive the motor with pulse-width modulation, given input analog signals between 0.0 and 10.0 V. The maximum control surface deflection is set to ±32 deg and establishes the minimum possible motor increment at 0.016 deg. The dynamics of the motor are neglected, and it is assumed that the motor reacts exactly as specified as long as the maximum rate of 4.75 rad/s is not achieved. The aerodynamics are slightly affected by placing the motor externally on the wing—the positive stall angle has been reduced from 16 to 13 deg, and the negative stall angle has been reduced from 16 to 15 deg.

Two U.S. Digital E-2 Optical Encoders are used to measure the plunge and pitch positions. These encoders are mounted on the pitch and plunge cams. Three data acquisition boards (a Data Translation® 2821-F16SE board, a Computer Boards'® CIO-CTR5 board, and a Computer Boards'® DIO-24H board), which perform all required operations, are used. Figure 3 shows the process flow of the system. The observer and full-state feedback efforts presented herein represent only one portion of the data acquisition and control system's capabilities.[22]

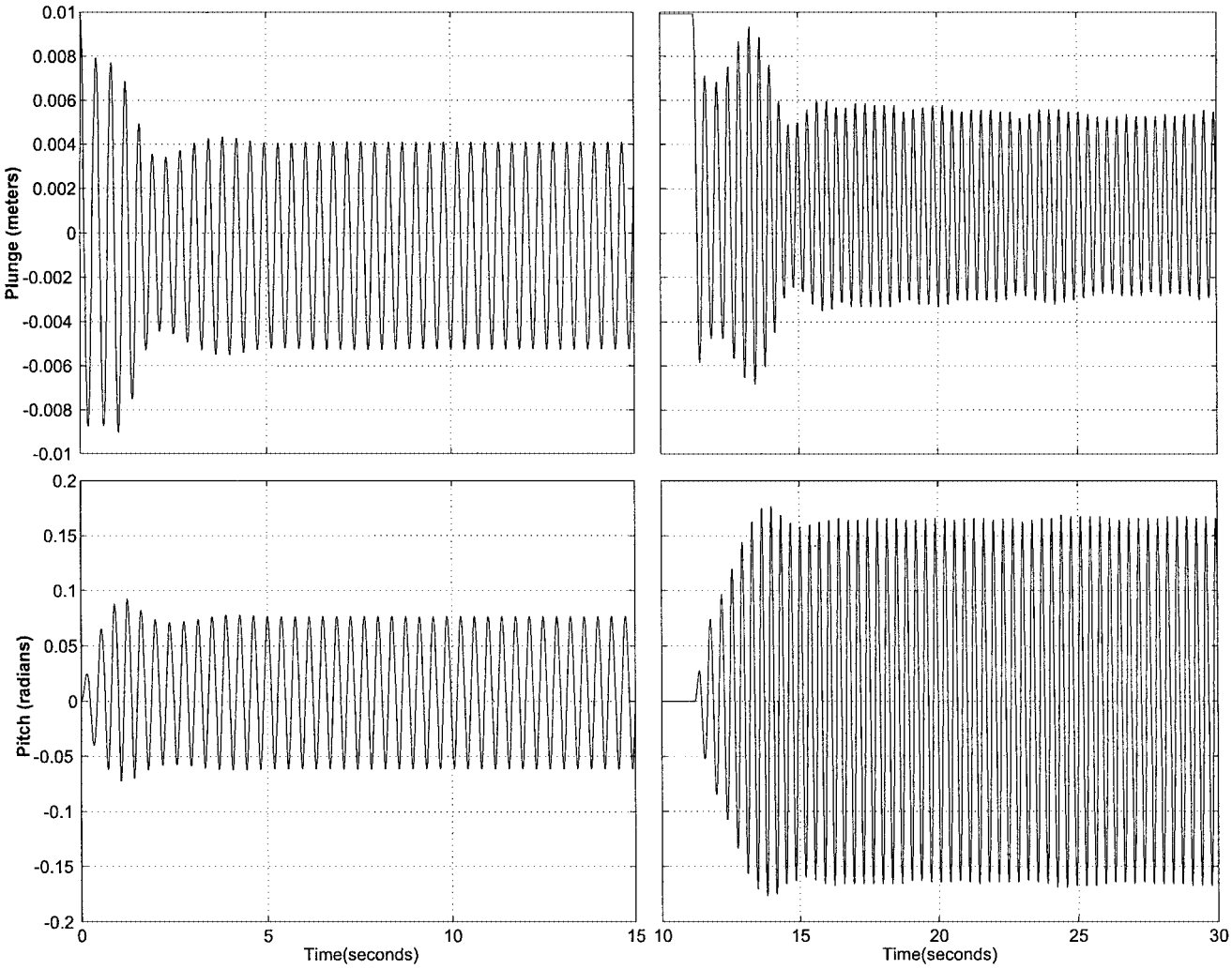

Fig. 6 Predictions of LCO response for the nonlinear system at u_∞ = 14.25 m/s are shown in the left-side view. Measurements of LCO response are shown in the right-side view.

The observer uses both the desired control signal and the measurements from the data acquisition system. A Runge–Kutta scheme is used to integrate the observer equations of motion, yielding position values that are a smoothed representation of the actual measurements as well as the 10 estimated states. All 12 calculated states are multiplied by the feedback gains to yield the control surface deflection. These values are converted to voltages and sent to the control surface for feedback.

Results

Analytical Results

Figure 4 shows the aerodynamic sensitivity of the roots of the open-loop system as the velocity is raised to 66.7 ft/s (20.0 m/s). The plot shows the system eigenvalues at 1.67 ft/s (0.5 m/s) increments of velocity for the elastic axis location of $a = -0.8424$. The pitch mode is unstable; the remaining modes are stable and satisfy the requirements that they are stabilizable and detectable. Because the only unstable mode is the pitch mode, LQR theory is used to derive controller gains for full-state feedback.

Also from Fig. 4, the flutter velocity and frequency are identified where the pitch mode has zero damping. The predicted flutter velocity and frequency are found to be 50.83 ft/s (15.25 m/s) and 2.07 Hz, respectively. All control laws are derived at 63.53 ft/s (19.06 m/s) or 25% above the flutter velocity. The weightings are chosen to normalize the maximum values of the measured variables. It is noted that a quicker response time is achieved by increasing the weighting for the plunge mode. A maximum displacement of 0.017 ft (0.005 m) for the plunge mode is used. Process noise estimates, proportional to the roots, are created to derive the observer feedback gains. Measurement noise is the square of the smallest possible measurements of the plunge and pitch motion, defined by the resolution of the optical encoders used in the experiment. With observation and full-state feedback, the system should be stabilized well above the flutter velocity.

Figure 5 shows the predicted plunge and pitch motion given a −0.0034 ft (−0.001 m) plunge and 0.09-rad pitch initial condition. The freestream velocity is 51.66 ft/s (15.5 m/s), which is immediately above the flutter velocity. Closed-loop control is initiated before aerodynamic stall occurs. Suppression of flutter by control is evident as the motion is stabilized within 2.0 s. Commanded control surface deflection is also shown. The control surface deflection is initially zero but responds to meet the required control signal. As the freestream velocity is raised, the settling time improves because the control surface has more authority.

A Runge–Kutta integration scheme is used for simulating the wing motion with the nonlinearities. Predictions for flutter velocity and frequency are 49.67 ft/s (14.9 m/s) and 2.02 Hz, respectively. The response of the system at critical flutter velocities is affected by the nonlinear pitch stiffness. The system response does not grow exponentially when the flutter velocity is reached; rather, LCOs occur. These LCOs are evident at velocities immediately below the open-loop flutter velocity and are dependent upon the initial conditions. Figure 6 shows the predicted LCOs given a 0.033-ft (0.01-m) initial condition in plunge, at a freestream velocity of 46.75 ft/s (14.25 m/s). The frequency of motion for the system is 2.70 Hz. Similar predictions occur for various initial conditions in pitch and/or plunge, and slight changes in velocity and frequency are due to the presence of Coulomb damping.[22]

Experimental Results

Several experiments are performed to measure the flutter velocity and frequency, as well as the control authority provided by the control surface. To find the flutter velocity, the freestream velocity is slowly increased and fixed at intervals. Plunge and pitch motion for various initial conditions are examined to identify aeroelastic response. At zero wind-tunnel velocity, the plunge natural frequency is 2.41 Hz and the pitch natural frequency is 1.55 Hz. As expected, there is a coalescence of frequencies as the wind-tunnel velocity is increased. For the elastic axis location of $a = -0.8424$, the frequencies coalesce to 2.10 Hz at the flutter velocity of 51.67 ft/s (15.5 m/s). These results agree well with the predicted results in Fig. 4.

The complete unsteady aerodynamic observer and controller system was built and tested, and several experiments for the linear system were performed to validate the model. Three primary sets of experiments were conducted and distinguished by the initiation of the control system. The first experiments (type 1) allowed control and estimation to begin while the response was growing. The second experiments (type 2) initiated control and estimation when the structure was released. The third experiments (type 3) allowed control and estimation to begin before release or disturbance.

Type 1 experiments were performed near the critical flutter velocity. If the velocity is much higher, the motion grows too rapidly to initiate control. These results show that as long as the motion does not exceed aerodynamic stall before starting the control, the system is always controllable. Measurements of plunge and pitch responses, as well as control surface motion, are presented in Fig. 5.

Comparisons between predictions and measurements (Fig. 5) of the controlled response of the linear (constant stiffness) system show good agreement in frequency of response. Before the activation of control, the trends associated with growth of motion and amplitude of response suggest that structural damping—namely, Coulomb damping—is improperly characterized. Our results indicate a high sensitivity of Coulomb damping to flowfield conditions and initial conditions.

Following the actuation of control, predictions and measurements show flutter suppression within 2 s. Again, trends associated with decay of motion and amplitude of response are due to the structural damping model. The control system is shown to stabilize at velocities over 100% above the open-loop flutter velocity.

As found through the type 2 experiments, less control surface motion is required at velocities above the flutter velocity. For these experiments, the freestream velocity is fixed, an initial condition is set for the pitch or plunge position, and the controller is started as the system is released from the initial conditions. Suppression is achieved for velocities up to 104.67 ft/s (31.4 m/s), but typically tests are not performed at these higher velocities to avoid exceeding limitations of the servomotor or structure.

As found through type 3 experiments, the system is extremely stable when control is started before release of the structure. Except for initial conditions that lead to aerodynamic stall, the system is always stabilized. Again, the system is tested up to 104.67 ft/s (31.4 m/s) but exhibits a more rapid settling time than those shown in the type 2 experiments. When the system is released, the control surface is already at the ideal position for stabilizing the system. For brevity, the measurements of type 2 and type 3 experiments are not presented herein but are described in detail by Block.[22]

From the experimental data, the linear control model is shown to be very effective. Before testing this controller on the nonlinear model, LCO boundaries must be determined. LCOs are due to the nonlinear pitch stiffness and are encountered at different velocities depending upon the initial conditions. Two initial conditions are used for these tests. With a 0.033-ft (0.01-m) plunge input, LCOs are initially encountered at approximately 47.5 ft/s (14.25 m/s) and a frequency of 2.87 Hz as presented in Fig. 6. With a 0.087-rad pitch input, LCOs occur at approximately 50.83 ft/s (15.25 m/s) and a frequency of 2.87 Hz.

Comparisons between the predictions and measurements of LCO behavior (Fig. 6) for the nonlinear system show good agreement in frequency of response and associated trends. As found in the linear results, differences in amplitude of response are due to the structural damping model.

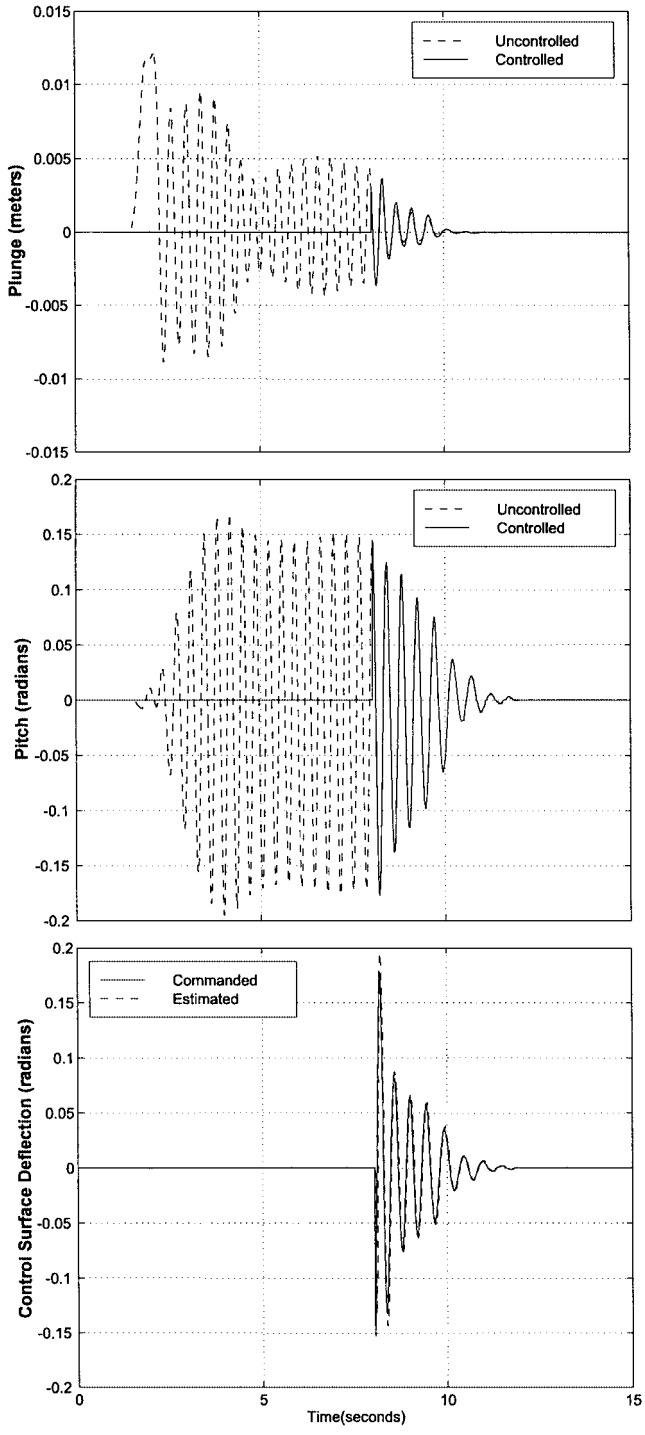

Fig. 7 Measurements of controlled response of LCO behavior for the nonlinear system at u_∞ = 16.0 m/s are shown. Top and middle views show plunge and pitch response. Bottom view shows control surface deflection.

The linear controller performs well as long as the system does not enter into LCO response before the initiation of control. However, when the system is experiencing LCO behavior, the single actuator controller has a limited ability to uncouple motion. The result of this controller action is a stabilized plunge motion and a larger amplitude (and frequency) pitching motion. When the system is in LCO motion, the coupling appears different to that of the linear flutter motion. It is observed that during flutter the plunge and pitch motion are 180 deg out of phase, but during LCOs the two motions are in phase. To stabilize the nonlinear system, a modified control law is required to address this phase difference. Herein, LCO control is only achieved near the flutter velocity. Figure 7 shows a case of control for LCO conditions; however, at higher velocities the present control law will not suppress the instability.

Conclusions

A nonlinear aeroservoelastic model is derived with an unsteady aerodynamic model using the Jones approximation to Theodorsen's function. This aerodynamic model is appropriate for the low reduced frequencies and low subsonic Mach numbers of the experiment. Two damping models are examined—viscous and Coulomb. In addition, the structural response of the model support system is tailored for a linear or nonlinear response through a cam system providing prescribed stiffness. The predictions for the open-loop system are in good agreement with the experiment measurements. Good correlation of predictions and measurements for the nonlinear aeroelastic model is also achieved. This correlation includes velocity, frequency, and amplitude of aeroelastic behavior. Differences between predictions and measurements are attributed to difficulties in modeling structural damping. Small differences are attributed to the presence of the servomotor in the flowfield and the inertial loads introduced by the servomotor that are not accounted for in the model.

With the experience gained from the initial experiments, an improved feedback system is developed. A trailing-edge control surface added to the existing wing structure and a high torque servomotor adapted to drive the surface lead to an aeroelastic control system capable of stabilizing the structure at velocities over twice the open-loop flutter velocity. The controller stabilizes the system for linear or nonlinear response. For a system undergoing LCO response, limited control is achieved by modifying the control law to account for phase characteristics. The aeroelastic control system developed for the wind-tunnel experiment performs well for cases in which control is initiated before LCO response. However, the control system is limited to the vicinity of open-loop flutter velocities if control is initiated following the onset of LCO response.

References

[1]Lyons, M. G., Vepa, R., McIntosh, S. C., and DeBra, D. B., "Control Law Synthesis and Sensor Design for Active Flutter Suppression," *Proceedings of the AIAA Guidance and Control Conference*, AIAA, New York, 1973, pp. 1–29 (AIAA Paper 73-832).

[2]Mukhopadhyay, V., Newsom, J. R., and Abel, I., "A Direct Method for Synthesizing Low-Order Optimal Feedback Control Laws with Application to Flutter Suppression," *Proceedings of the AIAA Atmospheric Flight Mechanics Conference*, AIAA, New York, 1980, pp. 465–475 (AIAA Paper 80-1613).

[3]Gangsaas, D., Ly, U., and Norman, D. C., "Practical Gust Load Alleviation and Flutter Suppression Control Laws Based on LQG Methodology," AIAA Paper 81-0021, Jan. 1981.

[4]Karpel, M., "Design for Active Flutter Suppression and Gust Alleviation Using State-Space Aeroelastic Modeling," *Journal of Aircraft*, Vol. 19, No. 3, 1982, pp. 221–227.

[5]Horikawa, H., and Dowell, E. H., "An Elementary Explanation of the Flutter Mechanism with Active Feedback Controls," *Journal of Aircraft*, Vol. 16, No. 4, 1979, pp. 225–232.

[6]Heeg, J., "Analytical and Experimental Investigation of Flutter Suppression by Piezoelectric Actuation," NASA TP 3241, Sept. 1993.

[7]Lin, C. Y., "Strain Actuated Aeroelastic Control," M.S. Thesis, Dept. of Aeronautics and Astronautics, Massachusetts Inst. of Technology, Cambridge, MA, Feb. 1993.

[8]Lazaraus, K., Crawley, E., and Lin, C., "Fundamental Mechanisms of Aeroelastic Control with Control Surface and Strain Actuation," *Journal of Guidance, Control, and Dynamics*, Vol. 18, No. 1, 1995, pp. 10–17.

[9]Lazarus, K., "Multivariable High-Authority Control of Plate-Like Active Lifting Surfaces," Ph.D. Dissertation, Dept. of Aeronautics and Astronautics, Massachusetts Inst. of Technology, Cambridge, MA, June 1992.

[10]Chen, P., Sarhaddi, D., and Liu, D., "Limit-Cycle-Oscillation Studies of a Fighter with External Stores," *Proceedings of 39th AIAA/ASME/ASCE/AHS/ASC Structures, Structural Dynamics, and Materials Conference*, AIAA, Reston, VA, 1998, pp. 258–266 (AIAA Paper 98-1727).

[11]Stearman, R. O., Powers, E. J., Schwartz, J., and Yurkovich, R., "Aeroelastic Identification of Advanced Technology Aircraft Through Higher Order Signal Processing," *Proceedings of the 9th International Modal Analysis Conference*, Society for Experimental Mechanics, Bethel, CT, 1991, pp. 1607–1616.

[12]Woolston, D. S., Runyan, H. L., and Andrews, R. E., "An Investigation of Effects of Certain Types of Structural Nonlinearities on Wing and Control Surface Flutter," *Journal of Aeronautical Sciences*, Vol. 24, No. 1, 1957, pp. 57–63.

[13]Breitbach, E. J., "Effects of Structural Nonlinearities on Aircraft Vibration and Flutter," AGARD-R-665, North Atlantic Treaty Organization, Neuilly sur Seine, France, Jan. 1978.

[14]Tang, D. M., and Dowell, E. H., "Flutter and Stall Response of a Helicopter Blade with Structural Nonlinearity," *Journal of Aircraft*, Vol. 29, No. 5, 1992, pp. 953–960.

[15]Lee, B. H. K., and LeBlanc, P., "Flutter Analysis of a Two-Dimensional Airfoil with Cubic Nonlinear Restoring Force," National Aeronautical Establishment, Aeronautical Note 36, National Research Council (Canada) 25438, Ottawa, ON, Canada, Feb. 1986.

[16]Theodorsen, T., "General Theory of Aerodynamic Instability and the Mechanism of Flutter," NACA Rept. 496, National Advisory Committee for Aeronautics, Hampton, VA, 1935.

[17]Theodorsen, T., and Garrick, I. E., "Mechanism of Flutter: A Theoretical and Experimental Investigation of the Flutter Problem," NACA Rept. 685, National Advisory Committee for Aeronautics, Hampton, VA, 1940.

[18]Fung, Y. C., *An Introduction to the Theory of Aeroelasticity*, Wiley, New York, 1955, pp. 207–215.

[19]Vepa, R., "On the Use of Pade Approximants to Represent Unsteady Aerodynamic Loads for Arbitrary Small Motions of Wings," *Proceedings of the AIAA Guidance and Control Conference*, AIAA, New York, 1976, pp. 1–12 (AIAA Paper 76-17).

[20]Edwards, J. W., Ashley, H., and Breakwell, J., "Unsteady Aerodynamic Modeling for Arbitrary Motions," *AIAA Journal*, Vol. 17, No. 4, 1979, pp. 365–374.

[21]O'Neil, T., "Experimental and Analytical Investigations of an Aeroelastic Structure with Continuous Nonlinear Stiffness," M.S. Thesis, Dept. of Aerospace Engineering, Texas A&M University, College Station, TX, May 1996.

[22]Block, J. J., "Active Control of an Aeroelastic Structure," M.S. Thesis, Dept. of Aerospace Engineering, Texas A& M University, College Station, TX, May 1996.

[23]Sage, A. P., and White, C. C., *Optimum Systems Control*, Prentice–Hall, Englewood Cliffs, NJ, 1977, pp. 191–230.